Chinese Chemical Letters 34 (2023) 108067

Contents lists available at ScienceDirect

Chinese Chemical Letters

journal homepage: www.elsevier.com/locate/cclet

Overriding the inherent alkalinity to dual phosphinito bimetallic catalyst for C(sp^2)-C(sp^3) formation: A combined computational and experimental study

Sujuan Zheng [a], Heng Zhang [a], Qian Peng [a,b,*]

[a] State Key Laboratory of Elemento-Organic Chemistry, Tianjin Key Laboratory of Biosensing and Molecular Recognition, Frontiers Science Center for New Organic Matter, College of Chemistry, Nankai University, Tianjin 300071, China
[b] Haihe Laboratory of Sustainable Chemical Transformation, Tianjin 300192, China

ARTICLE INFO

Article history:
Received 8 October 2022
Revised 9 December 2022
Accepted 12 December 2022
Available online 16 December 2022

Keywords:
Ni-Al bimetallic catalysis
Secondary phosphine oxides
Redox dehydrogenation
Dual-SPO model

ABSTRACT

Unraveling the catalytic reaction mechanism is a long-term challenge for developing efficient catalysts. The blooming bimetallic catalyst have enabled to activate inert bonds and realize complex C-C formation. Herein, we theoretically discover a dual-phosphinito bridged hetero-bimetallic species that verified by NMR experiments. Our results indicate only dual-phosphinito Ni-Al model can be an active catalyst in asymmetric cycloadditions *via* C-C activation and C-H activation, which can well rationalize the experimental observations for both reactivity and stereo-selectivity. An unprecedented tandem redox dehydrogenation mechanism was revealed to control the formation of this active species overriding the inherent basicity. Synergistic Lewis acid and e_g orbital interactions, including d_{z^2} orbital reoccupation and $d_{x^2-y^2}$ orbital recombination, were disclosed to understand both thermodynamic and kinetic advance of dual-bridged model, displaying feasible redox properties.

Bimetallic catalysis is a rising catalytic strategy for challengeable C-C bond formations together with enantio-control nowadays [1–6]. The development on new bridged ligands have greatly promoted the field of bimetallic catalysis to improve the reactivity and selectivity [7–11]. Secondary phosphine oxides (SPOs) have recently attracted more attention as robust pre-ligands for transition-metal catalysis (Scheme 1a) [12–16], especially for the bifunctional coordination (P and O) bridging two metals that may lead to the unknown synergistic effect for catalysis [5,6]. Due to the air- and moisture-tolerance, the secondary phosphine oxides (SPO) are useful and crucial reagents [17–19]. Ackermann *et al.* have made a remarkable progress in transition-metal catalysis and realized a series of cross coupling reactions [15,20]. Cramer [5] and Ye [6, 21-23] further developed this important field to Ni-Al hetero-bimetallic catalysis probably bridged by isomerized SPO. However, the NMR studies for the tautomeric behavior of various SPOs showed that P^V tautomer still predominates at ambient temperature [24], seemly suggesting the quick SPO tautomerism from P^V to P^{III} might not be true in reported reactions. Preliminary computational studies revealed direct intramolecular tautomerism [25,26] can be slightly lowered by Brønsted acid through intra- or inter-molecular proton shuttles (Scheme 1b) [27,28]. An alternative way to activate SPO is deprotonation by DBU [29], but the resulting transient P^{III} intermediate would not be stabilized and finally transformed a new P^V product.

Computational mechanistic studies for Ni catalyzed organic reactions had been revealed for rationalizing the experimental observations, such as reductive coupling [30], cross-coupling [31–34], photoredox catalysis [35,36]. Despite these impressive advances, hetero-bimetallic catalysis remains challenge and unsolved problem due to the complex redox and electronic structures of variable SPO ligand-mediated transition metal catalysts. Here, we disclosed a new dual-phosphinito bridging Ni-Al bimetallic species and addressed the catalytic mechanism. (1) How to form the on-site hetero-bimetallic complex? Tandem redox dehydrogenation mechanisms have been discovered together with an abnormal basicity (Scheme 1c). (2) What is the origin and driving force for bimetallic complex bridged by isomerized SPO? The synergistic effect of Lewis acid and e_g orbital interaction (LES) was raised. (3) Could the thermodynamic stable species be kinetically active? The dual-phosphinito bridged Ni-Al complex (dual-SPO) is an active catalyst shown in Scheme 1c, which is structurally similar to bio-mimic catalyst like double thio-bridged nickel-iron hydrogenase in biological chemistry [37]. Further NMR experiments and computational

* Corresponding author.
E-mail address: qpeng@nankai.edu.cn (Q. Peng).

https://doi.org/10.1016/j.cclet.2022.108067
1001-8417/

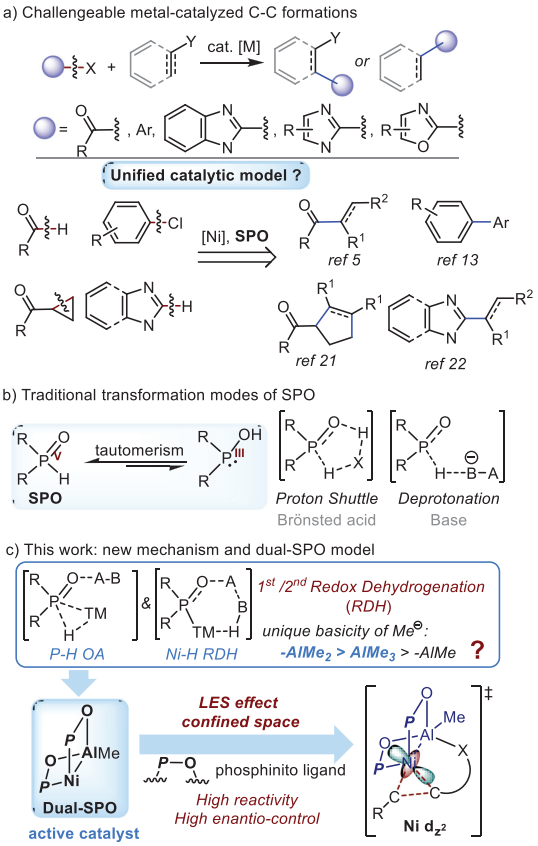

Scheme 1. Synthetic applications and secondary phosphine oxides (SPOs) transformation.

studies provided more evidences and applications for this novel model in this work.

Tautomerism from P^V to P^{III} is a well-accepted mechanism for SPO transformation [38]. However, our initial calculations indicate the reactivity of intermolecular H-transfer may vary from different substituents as shown in Fig. 1a. The tautomerism of SPO with electro-withdrawing group -CF_3 is relatively facile through the intermolecular proton shuttle (28.7 kcal/mol) probably due to the polarized P-H bond. Other SPOs with electro-donating substituents fail to undergo this tautomerism with more than 35 kcal/mol energy barriers. It is incomprehensible that many transition metal catalyzed reactions were achieved by using the P^{III} form of SPO with the electro-donating substituents [5,6,13,14,16,21,22]. There are six possible mechanisms for $Ph_2P(O)H$ transformation in order to rationalize SPO ligand role, including the self-assisted model, Brønsted acid assisted model, base ($AlMe_3$) assisted model, and transition metal (Ni) assisted model as shown in Fig. 1b (Fig. S1 in Supporting information). The intramolecular 1,2-H shift is prohibited by inherent high activation barrier in mode 1 no matter if it is activated by Lewis acid. The water or a second SPO molecule as Brønsted acid can facilitate this transformation through a proton shuttle (synergistic mechanism), but it still has to overcome more than 35.0 kcal/mol energy barrier (mode 2 and mode 3) [27,28]. The dehydrogenation process will occur by using $AlMe_3$ reagent in mode 4, and the methyl anion as strong Lewis base can lower the activation barrier to 25.3 kcal/mol, accelerating the $Ph_2P(O)H$ transformation. Moreover, SPO transformation *via* the P-H activation could also be realized by transition metal in the way of oxidative addition [39]. In the mode 5, the oxidative addition of P-H bond is quite favorable, but the slow hydrogen transfer from Ni to P=O blocks this transformation. To solve this problem, we raise a reductive dehydrogenation (RDH) model that is a distinct SPO

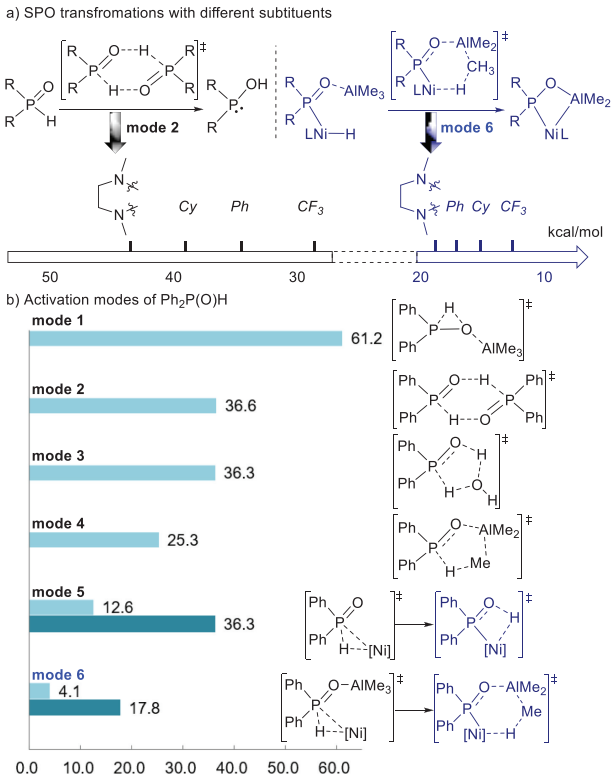

Fig. 1. Multiple activation modes of SPO transformation from P^V to P^{III}.

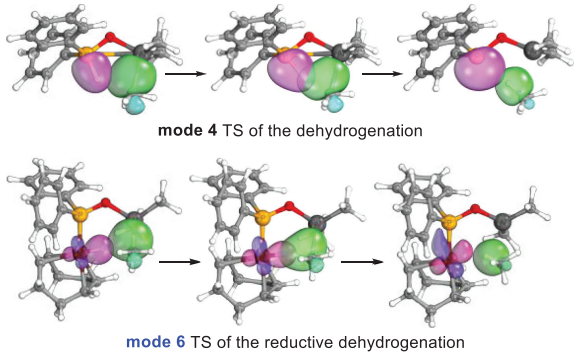

Fig. 2. Intrinsic bond orbitals (IBO) analysis along the intrinsic reaction coordinate (IRC) of the transition state of mode 4 and mode 6 at the PBE/def2-TZVP level of theory (Fig. S7 in Supporting information).

transformation mechanism combined modes 4 and 5, displaying the lowest energy barrier 17.8 kcal/mol (mode 6 of Fig. 1b). The reductive dehydrogenation *via* six-membered-ring transition state inherits the advantages of strong alkalinity of methyl anion in $AlMe_3$ and redox properties of Ni. And the bridging SPO ligand seemly balanced the hetero-bimetallic complex displaying the key catalytic function.

Then the intrinsic bond orbitals (IBOs) analysis were conducted to obtain the actual electron flow along the intrinsic reaction coordinate (IRC) of transition state for both mode 4 and mode 6. The pathway of mode 4 in Fig. 2 clearly illustrated the electron transfer from P-H bond to P lone pair, suggesting the P was reduced. And the IBOs analysis of the mode 6 indicated that σ orbital of Al-C would first donate electrons to the Ni-H bond, and then electrons of the Ni-H σ orbital in the transition state were gradually transferred to the $d_{x^2-y^2}$ orbital of Ni atom at the square planar coordination. Due to the key redox contribution of Ni, mode 6 of SPO transformation are tandem redox dehydrogenation mech-

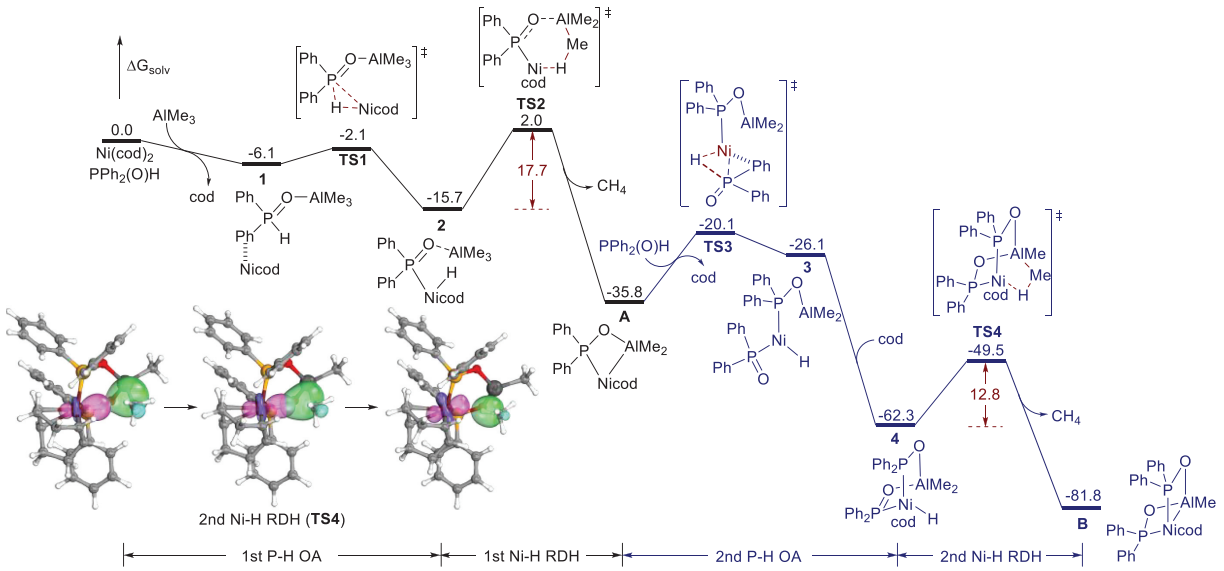

Fig. 3. The free energy profile for multistage activation of $Ph_2P(O)H$ in tandem redox dehydrogenation pathway of mode 6 and IBO analysis of TS4 (Fig. S7). The single-point energies were computed in mesitylene solvent. Energies in kcal/mol, the same below, unless otherwise specified.

Table 1
Dominant ^{31}P NMR signals of reactions for different ratios of $Ph_2P(O)H$, $AlMe_3$ and $Ni(cod)_2$.[a]

Entry	Ratio	Time[b]	^{31}P NMR (ppm)
1	1:1:1	1 h	95.7
2	2:1:1	1 h	95.7
3	2:1:1	3 d	95.7
4	3:1:1	1 h	95.7 (major), 18.9 (minor), 97.5 (minor)

[a] See Supporting information for the ^{31}P NMR spectra.
[b] Stirring and processing time.

anisms. The favorable model 6 can be applied to more SPOs with different substituents, showing pronounced energy advantage as shown in mode 6 (Table S2 and Fig. S2 in Supporting information). These comparable low energy barriers would fulfill the requirement of transition-metal catalysis mediated by SPO [5,6,13,21].

Under the redox dehydrogenation mechanism (model 6), a novel dual-phosphinito bridged Ni-Al intermediate was discovered through our computational study and also verified by our NMR research. A detailed mechanistic pathway was shown in Fig. 3. $Ph_2P(O)H$ easily undergoes P-H oxidative addition and Ni-H RDH *via* **TS1** and **TS2**, respectively, to form mono-phosphinito bridged Ni-Al intermediate **A** (mono-SPO), regenerating the active Ni^0. However, the reaction may not rest in the intermediate **A**, and potentially involves the second $Ph_2P(O)H$ forming the dual-phosphinito intermediate **B**. The 2nd P-H oxidative addition from the intermediate **A** *via* **TS3** is facile (15.7 kcal/mol), resulting Ni-H species **3**. Then 2nd Ni-H RDH *via* **TS4** is even lower than that of 1st Ni-H RDH. And the IBOs analysis of the 2nd RDH indicated that σ orbital of Al-C would first donate electrons to the Ni-H bond, and then electrons of the Ni-H σ bond in the transition state were gradually transferred to the d_{z^2} orbital of Ni atom at the trigonal bipyramid coordination. The third $Ph_2P(O)H$ transformation is inhibited due to relative high energy barriers (Fig. S4 in Supporting information), thus intermediate **B** would be a key resting state.

To seek experimental evidence of the intermediate **B**, ^{31}P-and ^1H NMR experiments were carried out to probe the reaction mechanism under different ratios of $Ph_2P(O)H$, $AlMe_3$ and $Ni(cod)_2$ shown in Table 1. Interestingly, the dominant signal observed in all of our ^{31}P NMR tests was a single peak at 95.7 ppm (entries 1-3), suggesting a strong driving force to form this intermediate regardless of compound ratios. And this signal is better

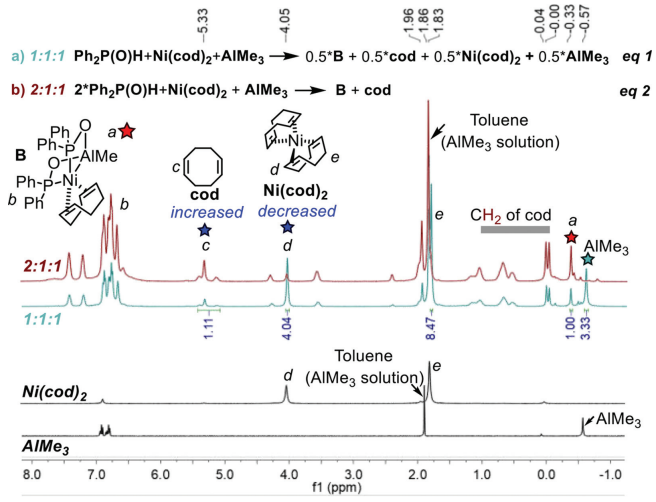

Fig. 4. ^1H NMR spectra of (a) reaction of 1:1:1 ratio of $Ph_2P(O)H$, $AlMe_3$ and $Ni(cod)_2$ for 1 h at room temperature, (b) reaction of 2:1:1 ratio of $Ph_2P(O)H$, $AlMe_3$ and $Ni(cod)_2$ for 1 h at room temperature. Spectra are referenced to tetramethylsilane (TMS).

to be assigned as intermediate **B** rather than **A**, because the intermediate **A** derived from single SPO transformation cannot explain the almost pure single peak in the 2:1:1 ratio of NMR test. And an unreacted $Ph_2P(O)H$ was supposed to be probed. Indeed, increasing the amount of $Ph_2P(O)H$ to 3:1:1 ratio would lead to extra two minor NMR signals at around 97.5 ppm and 18.9 ppm of ^{31}P NMR, which would be possible tri-phosphinito Ni-Al intermediates and excess unreacted $Ph_2P(O)H$, respectively (entry 4). However, dual-SPO remains the dominant of ^{31}P NMR (Fig. S8 in Supporting information). Our assignments were further supported by ^1H NMR with the comparisons of $AlMe_3$ and $Ni(cod)_2$ shown in Fig. 4. In the spectra of the mixture with the ratio of 1:1:1, the single peak at −0.33 ppm is assigned as -AlMe, and the ratio of its integral area to that of $AlMe_3$ at −0.57 ppm was close to 1:3, which is consistent with the corresponding stoichiometric equation shown in Eq. 1 of Fig. 4 assuming the formation of intermediate **B**. And the same -AlMe signal with seemly high concentration can also be observed in the ^1H NMR of 2:1:1 ratio mixture, together with the trivial signal for $AlMe_3$ (Eq. 2).

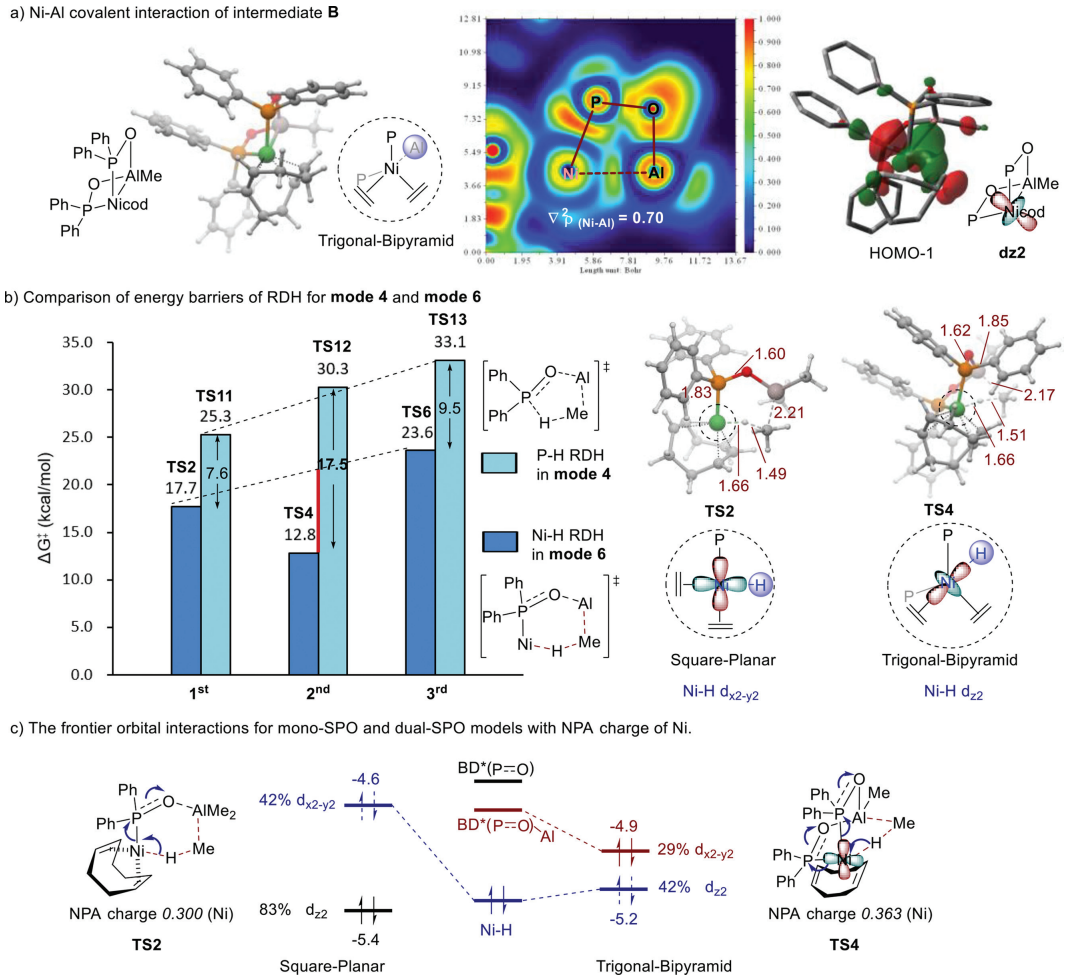

Fig. 5. (a) The calculated structure of intermediate **B** with Ni-Al interaction. The ELF value between Ni and Al atoms was 0.7 a.u., indicating that the important covalent interactions. (b) Comparison of energy barriers of RDH for mode 4 and mode 6. Calculated structures of **TS2** and **TS4** in mode 6. (c) The frontier orbital interactions for mono-SPO and dual-SPO models with NPA charge of Ni (energies in eV).

Moreover, the increased intensity of free cod signal "*c*" and the decreased intensity of $Ni(cod)_2$ signal "*d*" provided another evidence to support the Eqs. 1 and 2, suggesting the formation of dual-SPO intermediate **B**.

The DFT calculations indicated dual-SPO intermediate **B** is a trigonal bipyramidal structure with the apical Al coordination (Fig. 5a). There is a non-negligible Ni-Al covalent interaction in **B**, which can be demonstrated from the electron localization function (ELF). The frontier orbital (HOMO-1) of Ni's d_{z^2} electrons donated to 3p vacant orbitals of Al, suggesting the Ni(0) can be stabilized by Lewis acid Al^{III}. This donor-acceptor interaction could be an important thermodynamic driving force to form dual-SPO **B** (Fig. 3), which also provides insights into the mechanistic model for Ni-Al bimetallic catalysis [40–42]. To reveal the origin of control for dual-SPO **B**, the multiple stage of SPOs transformation for mode 4 in Fig. 1b were introduced for comparisons (Fig. S3 for detailed free energy profiles in Supporting information). Unlike the direct dehydrogenation of mode 4, transition metal Ni in redox dehydrogenation mode 6 makes the P-H bond of SPO convert to the activated Ni-H bond *via* P-H oxidative addition, and then Ni-H bond proceeds a favorable reductive dehydrogenation (Figs. 3 and 5b). There are inherent energy stabilizations between P-H RDH and Ni-H RDH (energy difference between two dotted lines). In contrast to the usual increasing energy trend in mode 4, an extra energy decreasing from 1st to 2nd Ni-H RDH of mode 6 seems override the nature basicity ($-AlMe_2$ > $AlMe_3$ > -AlMe), which could be attributed to different redox properties of the d orbitals of transition metal Ni. As shown in the stereo-structures in Fig. 5b, two transition states of 1st and 2nd Ni-H RDH have different spatial configurations of Ni-H. The stable **TS4** of 2nd Ni-H RDH formed a trigonal bipyramid coordination, and the apical hydride enable to interact with d_{z^2} orbital of Ni. While the square planar coordination can be found in the less stable **TS2** of 1st Ni-H RDH, and the planar hydride reoccupied to the $d_{x^2-y^2}$ orbital of Ni. IBO analysis in Figs. 2 and 3 can also indicate the $d_{x^2-y^2}$ and d_{z^2} orbitals of Ni operated in the dehydrogenation process, respectively. Therefore, the redox potential of Ni-H compensates the weak basicity of $-AlMe_2$, showing reductive basicity for the unusual trend of energy barriers. In Fig. 5c, the closely degenerate e_g orbital (d_{z^2} and $d_{x^2-y^2}$) in trigonal-bipyramid field of dual-SPO species would fulfil efficient electron reoccupation of Ni-H and the orbital recombination with anti-bond (P=O) (BD*) which was supported by relatively low *d* orbital component. That is in contrast to mono-SPO one in square-planar field (Fig. S6 in Supporting information). Moreover, the Lewis acid Al^{III} interaction with SPO can not only stabilize the BD* orbital to match the $d_{x^2-y^2}$ orbital in energy level, but also meet symmetry-adapted $d_{x^2-y^2}$ orbital rather than d_{z^2} orbital under the dual-coordination model (Fig. S5 in Supporting information). Therefore, the Lewis acid (L) and e_g (E) orbital interactions were synergetic (S) through the SPO linker that stabilized dual-SPO model for both kinetic and thermodynamic perspectives. This LES effect is particularly efficient for reductive process (*i.e.*, reductive dehydrogenation) with relatively high positive NPA charge on metal center in Fig. 5c.

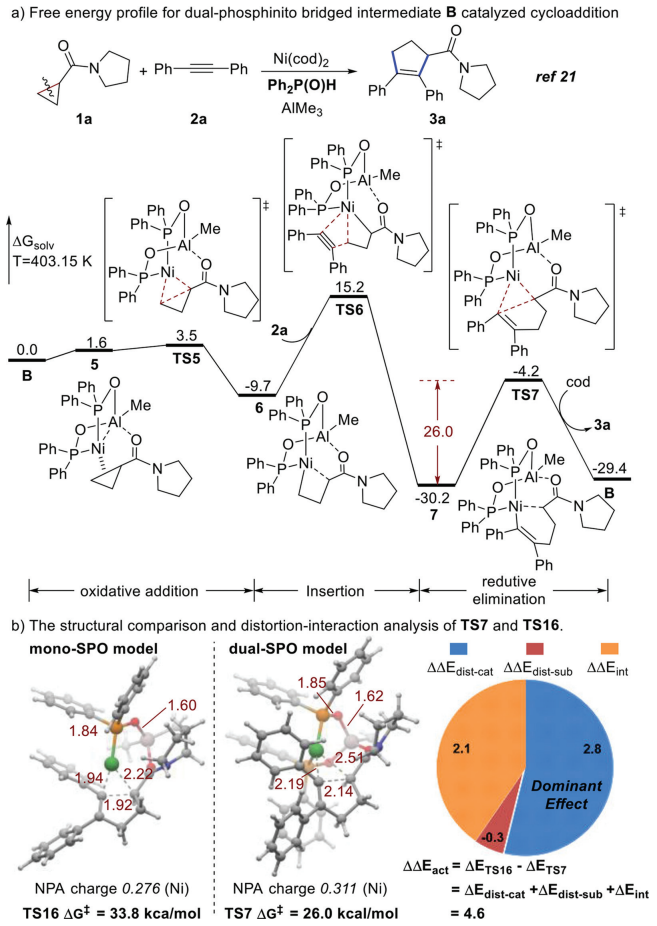

Fig. 6. (a) Free energy profile for dual-SPO B catalyzed cycloaddition of cyclopropyl carboxamide with alkyne. (b) The comparison of the reductive elimination transition state **TS16** and **TS7** in two models. The single-point energies were computed in mesitylene solvent.

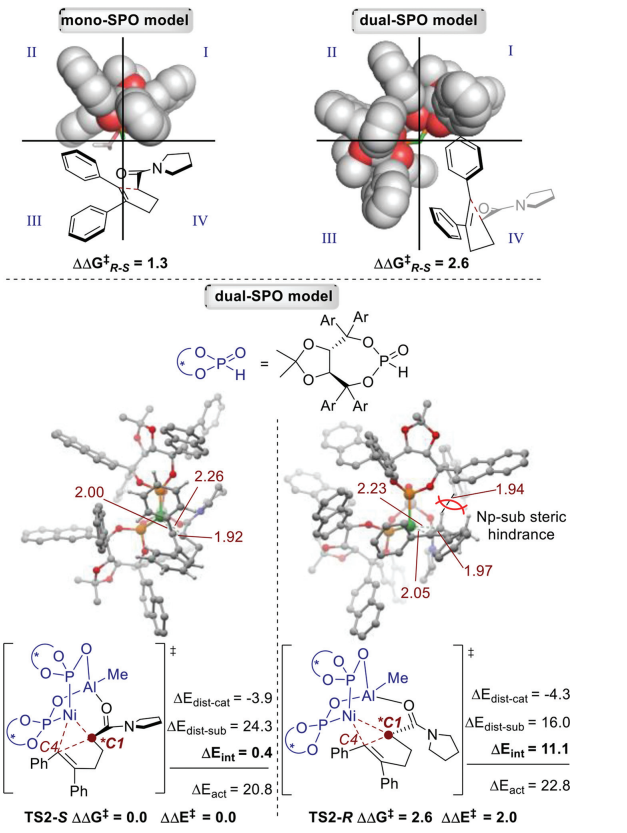

Fig. 7. Stereo-selective control model and transition states for reductive elimination step of asymmetric version.

The dual-SPO **B** can be an active catalyst and may promote the C-C reductive elimination under the control of LES effect, which rationalize the mechanism of more C-C forming reactions. An important case developed by Ye and coworkers is the asymmetric cycloaddition of cyclopropyl carboxamide with alkyne by using $Ni(cod)_2/Ph_2P(O)H/AlMe_3$ [21]. And reaction yields were highly depended on the ratio of $Ni(cod)_2$ and $Ph_2P(O)H$. The catalytic cycle consists of oxidative addition of C-C bond, alkyne insertion of Ni-C bond and reductive elimination, as shown in Fig. 6a. The calculated C-C bond cleavage is facile and reversible with low energy barrier, although it was supposed to be a difficult step [43,44]. After the irreversible alkyne insertion, the ring extension intermediate **7** were formed as a resting state for the following reductive elimination with a new $C(sp^2)$-$C(sp^3)$ bond formation. The reductive elimination was a turnover-limiting step with 26.0 kcal/mol to afford the product cyclopentenyl carboxamide **3a**, regenerating the catalytic species **B**. Compared with the reductive elimination transition state **TS16** mediated by mono-SPO **A** (Fig. S10 in Supporting information), **TS7** *via* dual-SPO model was favorable for 7.8 kcal/mol and formed an early transition state (Fig. 6b). Distortion-interaction analysis [45] demonstrates that the distortions of catalysts were the dominant factor, that is, the dual- phosphinito ligands between the Ni and Al display a 2.8 kcal/mol distortion energy more favorable than mono-phosphinito ligand (Fig. S13 in Supporting information). This could be attributed to the stable Ni-Al covalent interaction and rigid bridged conformation in catalytic species **B**, which may drive the reaction to release product **3a**. In addition, the favorable interactions between catalyst and substrate indicate that the LES effect of dual-SPO **B** also promotes the reductive elimination, supported by the stronger d_{z2} orbital interaction rather than the d_{x2-y2} interaction in mono-SPO **A** (Fig. S11 in Supporting information) and the more positive NPA charge (Fig. 6b). It is also consistent with our previous discussions of Ni-H reductive dehydrogenation process.

Our dual-SPO model can also well rationalize the asymmetric induction of cyclization under the chiral Taddol-derived SPO that precursor of P^{III} ligand (Fig. 7). The reductive eliminations here as the turnover-limiting step and enantio-determining step were 21.8 and 24.4 kcal/mol for *S*- and *R*-configuration, respectively (Fig. S12 in Supporting information). And the predicted *ee* value would be 92.8% ($\Delta\Delta G^{\ddagger} = 2.6$ kcal/mol) for *S*-product that is consistent qualitatively and quantitatively with experiment data (93% *ee*). We also examine the enantio-selectivity of mono-SPO model by using the same ligand (Fig. S12). Although it could qualitatively predict the *S*-product, the mono-SPO model cannot fulfil the reactivity and selectivity of the asymmetric cyclization due to the relatively high energy barrier and underestimated energy difference (1.3 kcal/mol) between *S*- and *R*-transition states. From stereo-structures of **TS2-*S*/*R*** and **TS3-*S*/*R***, the dual-phosphinito bridged Ni-Al catalyst, rather than mono-one, occupies the 3/4 quadrant of spatial region, which provides an advantage confined space for chiral induction [46]. Further structural analysis of the enantiomers in dual-SPO model suggests that more suitable space matches the *S*-configuration transition state (Fig. 7). And key ligand-substrate steric repulsions between naphthyl and methylene would lead to less stable interaction energy between the catalyst and substrate blocking the formation of *R*-product. Additional two chiral SPO ligands have been investigated as well (Fig. S16 in Supporting information) [5,23], which support the dual-SPO model showing the better reactivity and thermodynamic stability. And thus our model may be accessible and suitable for more asymmetric reactions.

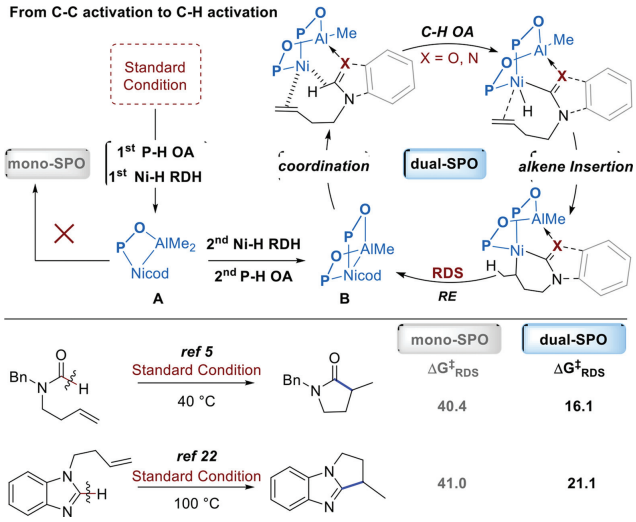

Scheme 2. More applications of dual-SPO model for C-H activation to form C(sp^2)-C(sp^3) bond catalyzed by standard condition: 5 mol% $Ni(cod)_2$, 5 mol% SPO and 20-40 mol% $AlMe_3$.

Besides the C-C activation of the cyclopropane in carboxamide [21], C-H activations of formamides [5] and imidazoles [22] catalyzed by $Ni(cod)_2$/SPO/$AlMe_3$ were also calculated to unravel the catalytic mechanism as shown in Scheme 2. The dual-SPO model was predicted more favorable than mono-SPO model based on activation barriers of key intermediates and transition states, indicating suitable and reasonable applications of our discovered dual-SPO model (Figs. S14 and S15 for energy profile). The extremely high energy barriers of reductive elimination for mono-SPO models cannot be achieved under reaction conditions, suggesting the possible catalytic models from original papers should be revisited further. From the experimental point of view in Table S3 (Supporting information), the reasonable moderate/high yield can be achieved in the 1:2 ratio of $Ni(cod)_2$/SPO, and there is only slight effect for increasing additional SPO or $Ni(cod)_2$ catalysts, which may provide not only another support for our dual-SPO model, but a unique perspective to reduce the catalyst loading.

In summary, a dual-phosphinito bridged Ni-Al complex for bimetallic catalysis was revealed by quantum mechanics calculations, and demonstrated by ^{31}P NMR and ^{1}H NMR under the solution of $Ni(cod)_2$/SPO/$AlMe_3$. The tandem redox dehydrogenation mechanisms were discovered to form this hetero-bimetallic species through the relay SPO transformations, involving P-H bond oxidative addition and Ni-H reductive dehydrogenation. Importantly, this dual-SPO bridged complex **B** with the trigonal bipyramid coordination and Ni-Al covalent interaction is suggested to be the active catalyst, displaying the generality for several challenging catalyzed C-C formations. By overcoming the weak alkalinity of methyl anion in -$AlMe_2$, the dual-SPO model could effectively reduce the energy barrier of reductive process, which is attributed to the synergistic effect of Lewis acid and e_g orbital interactions (LES). The mechanism of asymmetric inductions provides further evidences that only dual-SPO model enables to predict the experimental enantioselectivity qualitatively and quantitatively. Our mechanistic scenario provides not only deep insights into the case studies of reactivity patterns of the Ni-Al active species, but also probably distinct perspectives for active catalysts of challengeable reactions.

Declaration of competing interest

The authors declare that they have no known competing financial interests or personal relationships that could have appeared to influence the work reported in this paper.

Acknowledgments

We thank Prof. Mengchun Ye and Prof. Xuncheng Su for discussions of NMR experiments. We gratefully acknowledge the National Key Research and Development Program of China (No. 2021YFA1500100), the National Natural Science Foundation of China (Nos. 92156017, 21890722, 22188101), the NSF of Tianjin Municipality (No. 19JCJQJC62300), Tianjin Research Innovation Project for Postgraduate Students (No. 2019YJSB081), and Haihe Laboratory of Sustainable Chemical Transformation of Tianjin for generous financial support.

Supplementary materials

Supplementary material associated with this article can be found, in the online version, at doi:10.1016/j.cclet.2022.108067.

References

[1] J. Park, S. Hong, Chem. Soc. Rev. 41 (2012) 6931–6943.
[2] Y.Y. Zhou, C. Uyeda, Science 363 (2019) 857–862.
[3] J. Campos, Nat. Rev. Chem. 4 (2020) 696–702.
[4] B.M. Trost, G. Zhang, M. Xu, X. Qi, Chem. Eur. J. 28 (2022) e202104268.
[5] P.A. Donets, N. Cramer, J. Am. Chem. Soc. 135 (2013) 11772–11775.
[6] J.F. Li, Y.X. Luan, M. Ye, Sci. China Chem. 64 (2021) 1923–1937.
[7] D. Brazzolotto, L. Wang, H. Tang, et al., ACS Catal. 8 (2018) 10658–10667.
[8] R. Srivastava, R. Moneuse, J. Petit, et al., Chem. Eur. J. 24 (2018) 4361–4370.
[9] N. Saito, J. Takaya, N. Iwasawa, Angew. Chem. Int. Ed. 58 (2019) 9998–10002.
[10] R.M. Charles, T.P. Brewster, Coord. Chem. Rev. 433 (2021) 213765.
[11] C. Guo, L. Su, D. Yang, B. Wang, J. Qu, Chin. Chem. Lett. 33 (2022) 217–220.
[12] N.V. Dubrovina, A. Börner, Angew. Chem. Int. Ed. 43 (2004) 5883–5886.
[13] L. Ackermann, Isr. J. Chem. 50 (2010) 652–663.
[14] T.M. Shaikh, C.M. Weng, F.E. Hong, Coord. Chem. Rev. 256 (2012) 771–803.
[15] D. Ghorai, J. Loup, G. Zanoni, L. Ackermann, Synlett 30 (2019) 429–432.
[16] J. Francos, D. Elorriaga, P. Crochet, V. Cadierno, Coord, Chem. Rev. 387 (2019) 199–234.
[17] X. Ye, L. Peng, X. Bao, C.H. Tan, H. Wang, Green Synth. Catal. 2 (2021) 6–18.
[18] H. Wang, H. Qian, J. Zhang, S. Ma, J. Am. Chem. Soc. 144 (2022) 12619–12626.
[19] Q. Lin, S. Zheng, L. Chen, et al., Angew. Chem. Int. Ed. 61 (2022) e202203650.
[20] L. Ackermann, R. Born, J.H. Spatz, D. Meyer, Angew. Chem. Int. Ed. 44 (2005) 7216–7219.
[21] Q.S. Liu, D.Y. Wang, Z.J. Yang, et al., J. Am. Chem. Soc. 139 (2017) 18150–18153.
[22] Y.X. Wang, S.L. Qi, Y.X. Luan, et al., J. Am. Chem. Soc. 140 (2018) 5360–5364.
[23] J.F. Li, D. Pan, H.R. Wang, et al., J. Am. Chem. Soc. 144 (2022) 18810–18816.
[24] A. Christiansen, C. Li, M. Garland, et al., Eur. J. Org. Chem. 2010 (2010) 2733–2741.
[25] M. Solà, A. Toro-Labbé, J. Phys. Chem. A 103 (1999) 8847–8852.
[26] S.S. Wesolowski, N.R. Brinkmann, E.F. Valeev, et al., J. Chem. Phys. 116 (2002) 112–122.
[27] B.G. Janesko, H.C. Fisher, M.J. Bridle, J.L. Montchamp, J. Org. Chem. 80 (2015) 10025–10032.
[28] D. Vincze, P. Abranyi-Balogh, P. Bagi, G. Keglevich, Molecules 24 (2019) 3859–3870.
[29] L. Gavara, C. Petit, J.L. Montchamp, Tetrahedron Lett. 53 (2012) 5000–5003.
[30] H. Wang, G. Lu, G.J. Sormunen, et al., J. Am. Chem. Soc. 139 (2017) 9317–9324.
[31] M.S. Cheung, F.K. Sheong, T.B. Marder, Z. Lin, Chem. Eur. J. 21 (2015) 7480–7488.
[32] S.Q. Zhang, B.L.H. Taylor, C.L. Ji, et al., J. Am. Chem. Soc. 139 (2017) 12994–13005.
[33] M. Cao, H. Xie, Chin. Chem. Lett. 32 (2021) 319–327.
[34] L. Liu, H. Wu, G. Huang, Chin. Chem. Lett. 32 (2021) 3015–3018.
[35] A. de Aguirre, I. Funes-Ardoiz, F. Maseras, Angew. Chem. Int. Ed. 58 (2019) 3898–3902.
[36] Y. Jia, Y.Y. Liu, L.Q. Lu, et al., CCS Chem. 4 (2021) 1577–1586.
[37] D. Basu, T.S. Bailey, N. Lalaoui, et al., Inorg. Chem. 58 (2019) 2430–2443.
[38] C.H. Wei, C.E. Wu, Y.L. Huang, R.G. Kultyshev, F.E. Hong, Chem. Eur. J. 13 (2007) 1583–1593.
[39] L.B. Han, N. Choi, M. Tanaka, Organometallics 15 (1996) 3259–3261.
[40] C.C. Tsai, W.C. Shih, C.H. Fang, et al., J. Am. Chem. Soc. 132 (2010) 11887–11889.
[41] T. Tamaki, M. Ohashi, S. Ogoshi, Angew. Chem. Int. Ed. 50 (2011) 12067–12070.
[42] Y. Nakao, E. Morita, H. Idei, T. Hiyama, J. Am. Chem. Soc. 133 (2011) 3264–3267.
[43] K.E. Ylijoki, J.M. Stryker, Chem. Rev. 113 (2013) 2244–2266.
[44] A.G. Amador, E.M. Sherbrook, T.P. Yoon, J. Am. Chem. Soc. 138 (2016) 4722–4725.
[45] D.H. Ess, K.N. Houk, J. Am. Chem. Soc. 129 (2007) 10646–10647.
[46] I. Coric, B. List, Nature 483 (2012) 315–319.